Microfluidic device for immunoassays based on surface plasmon resonance imaging

Yiqi Luo, Fang Yu and Richard N. Zare*

Received 14th January 2008, Accepted 11th March 2008
First published as an Advance Article on the web 28th March 2008
DOI: 10.1039/b800606g

We have designed and fabricated a polydimethylsiloxane (PDMS) microfluidic device containing an array of gold spots onto which antigens or antibodies of interest can be attached. We use surface plasmon resonance (SPR) imaging to monitor the antibody–antigen recognition and binding events. This combination offers two significant advantages: (1) the microfluidic device dramatically reduces reaction time and sample consumption; and (2) the SPR imaging yields real-time detection of the immunocomplex formation. Thus, an immunoreaction may be detected and quantitatively characterized in about 10 min. The sensitivity of this method is at the subnanomolar level. When gold nanoparticles are selectively coupled to the immunocomplex to cause signal amplification, the sensitivity reaches the ten to one hundred picomolar level but the time required increases to about 60 min.

Introduction

Immunoassays, such as the enzyme-linked immunosorbent assay (ELISA), have become one of the most powerful biochemical analysis techniques.[1,2] Traditionally, these assays are carried out without sample replenishment in microplates having submillilitre wells. Moreover, ELISA relies on an enzyme-conjugated secondary antibody to couple with the immunocomplex for generating signals for measurement. When analyzing samples in low quantity, ELISA often takes hours to complete. This long time is needed both for the multiple steps involved and for the need of each step to reach equilibrium. Moreover, sample consumption is at the submillilitre level, which for rare samples may present an important limitation.

Some reports have appeared describing the running of immunoassays in microfluidic devices employing various detections methods such as fluorometric and colorimetric measurement, thermal lensing, electrochemical detection, and surface plasmon resonance (SPR).[3–14] The microfluidic devices usually contain only a single or a set of parallel flow channels, which require sequential reagent loading steps for multi-step immunoassays. This feature limits their applications, especially when the detection method is sensitive to disturbance during the immunoassays. Therefore, we have designed and fabricated a microfluidic device with a format of crossed flow channels that can achieve sequential delivery of reagents with only one step of reagent loading. The microfluidic device is made of polydimethylsiloxane (PDMS) incorporating an array of thin gold spots. PDMS allows easy installation of flow-control valves because of its elasticity, and the gold spots are suitable for carrying out immunoreactions with SPR detection.

Department of Chemistry, Stanford University, Stanford, California, 94305-5080, USA. E-mail: zare@stanford.edu; Fax: +1-(650)-725-0259; Tel: +1-(650)-723-3062

The combination of a microfluidic device with SPR imaging[15,16] offers three significant advantages. (1) The microfluidic device provides flow channels with nanolitre volumes. This feature accelerates the immunoreactions because the reagents are quickly replenished by the liquid flow. (2) The use of microfluidics allows the immunoassay to be carried out with less sample consumption. (3) SPR imaging gives real-time monitoring of the immunocomplex formation by sensing the refractive index change of binding molecules to the surfaces of gold spots. The real-time detection makes it possible to monitor the results before an immunoreaction has reached equilibrium. Thus, an immunoreaction may be detected and quantitatively characterized in about 10 min, which might be compared to at least 60 min in traditional microplate immunoassays such as ELISA. The SPR imaging technique also allows a large detection region, on the order of several square centimetres, so that the functional modules in the microfluidic device may be copied in parallel for high throughput. Furthermore, a microfluidic device is well-suited for automation, which allows manipulations to be sequenced and computer-controlled for the efficiency and precision of the immunoassay. In what follows we present information for the construction of the combined microfluidic device and SPR imaging readout, and we illustrate its use by examining a model system. We monitor the binding of anti-biotin antibodies to surface-immobilized biotinylated bovine serum albumin, without and with an additional signal amplification step.

Experimental

Chemicals and reagents

All chemicals and reagents are obtained from commercial sources: bovine serum albumin (BSA), biotinylated BSA (biotin-BSA), anti-biotin monoclonal antibody produced in goat (anti-biotin Ab), anti-goat IgG antibody produced in rabbit labeled with gold nanoparticles (AuNP-Ab), methyltrichlorosilane

 This journal is © The Royal Society of Chemistry 2008

(MTCS) from Sigma–Aldrich (St. Louis, MO, USA); phosphate-buffered saline (PBS) at pH 7.4 from Invitrogen (Carlsbad, CA, USA); *n*-dodecyl-D-maltoside (DDM) from Anatrace (Maumee, OH, USA); and PDMS RTV 615 from GE (Fairfield, CT, USA); and photoresist SU-8 from MicroChem (Newton, MA, USA).

Layout of the microfluidic device

Fig. 1A shows a schematic diagram of the microfluidic device, which is composed of two layers. The lower layer, which is called the flow layer, is where the immunoreactions occur. It contains two sets of crossed flow channels (dark green lines and light green lines), each with a width of 100 μm and a height of ~10 μm. Two neighboring flow channels are connected to the same inlet and outlet reservoirs. This design permits four replications of each immunoreaction. The crossed flow channels allow two sets of reagents to be loaded in the reagent reservoirs and sequentially injected. This feature may eliminate one step of reagent loading during the immunoassay, which is beneficial for obtaining real-time SPR images of the microfluidic device. Flow channel intersections are designed to have a diameter of 200 μm. An array of circular gold spots (brown dots) with a diameter of 250 μm and a thickness of ~50 nm are located in the channel intersections. The gold spot diameters purposely overfill the flow channel intersections to avoid problems with misregistration. The gold spots are used as SPR sensing platforms for immunoreactions. An additional flow channel (pink line) serves to rinse the gold spots, as needed. All reservoirs (light green, dark green, and pink circles) are ~1.5 mm in diameter. The liquid flows are driven by pressure (dry nitrogen), which is conveyed through tubes connected to the reservoirs.

The upper layer, which is called the control layer, is where microvalves are placed, which are used to open or close the flow channels beneath. The horizontal and vertical flow channels are separately controlled by vertical valves (blue rectangles) and horizontal valves (red rectangles). The valves are actuated by pressure, which is conveyed through tubes connected to external openings (red and blue circles). In the control layer, the valves are 200 μm wide and 55 μm high. Fig. 1B shows a picture of a prototype microfluidic device, which is compared in size to a penny.

Fabrication of the microfluidic device

The microfluidic device is fabricated using layer-by-layer lamination of PDMS, which is attached to a gold-deposited glass slide. Fig. 2 outlines the process. The fabrication employs a PDMS dipping-attaching method reported elsewhere.[17] This method is not only used for the bonding PDMS layers but also for bonding PDMS to the glass slide.

For fabricating PDMS layers, photoresist masters are formed on 4 inch silicon wafers by photolithography to produce molds. The patterns are printed on transparency films with high-resolution (40 640 dpi). To make a mold for the flow layer, positive photoresist SPR 220–7 is spin-coated on a silicon wafer with a thickness of 10 μm and baked on a hotplate (95 °C for 200 s). The photoresist is exposed through the transparency mask and developed. The wafer is then baked in an oven (110 °C for 1 h) to reflow the photoresist so that round patterns are formed. To make a mold for the control layer, negative photoresist SU-8 is spin-coated on a silicon wafer with a thickness of 55 μm and baked twice (75 °C for 180 s and 105 °C for 360 s). The photoresist is exposed through the transparency mask, post-baked twice (75 °C for 60 s and 105 °C for 300 s) and developed. The molds are exposed to MTCS vapor in a desiccator in order to prevent adhesion between PDMS and the molds.

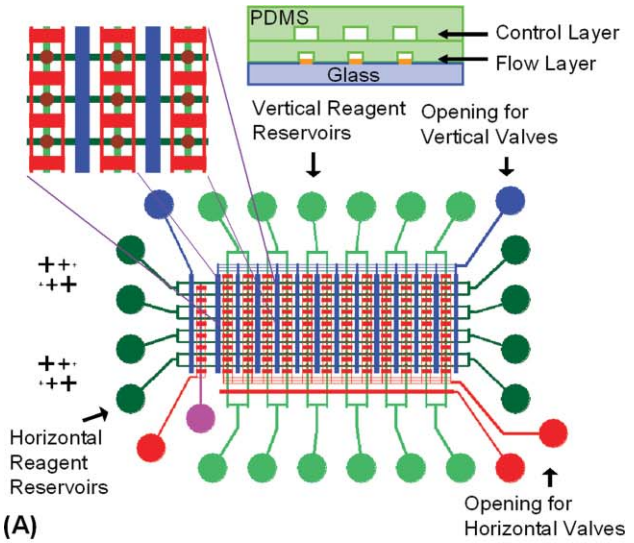

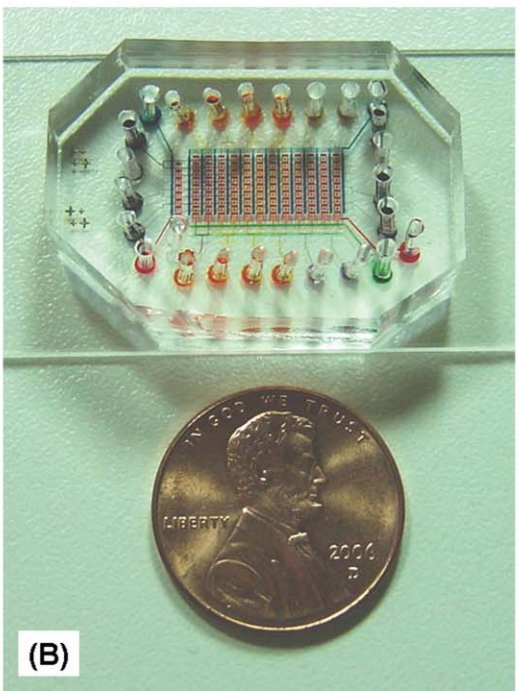

Fig. 1 (A) Layout of the microfluidic device. The structure of flow channels and valves are enlarged at the top-left corner, in which valves (red and blue rectangles) in the control layer are aligned onto the flow channels (light and dark green lines) in the flow layer. Gold spots (brown dots) are located at the intersections of the flow channels. The cross-sectional view of the microfluidic device shown on the top displays the vertical positioning of the control and flow layers in which green is used for denoting PDMS and blue for glass. (B) Picture of a prototype microfluidic device in which valves and flow channels are filled with food colorings for easy visualization. A penny serves as a size marker.

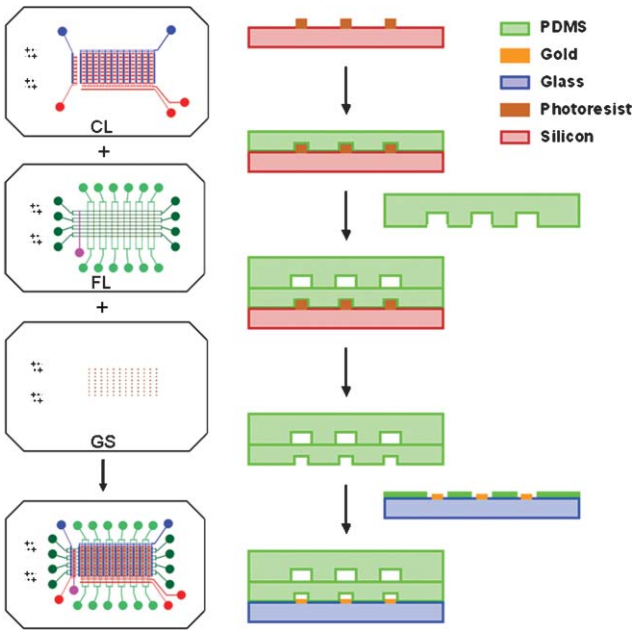

Fig. 2 Scheme of layer-by-layer lamination (left) and procedure of fabrication (right) of the microfluidic device. CL denotes the control layer, FL the flow layer, and GS the glass slide with gold spots.

The control layer is made by pouring PDMS prepolymer (mixture of RTV A and B with a mass ratio of 10 : 1) on the mold to a thickness of ~1 cm and curing PDMS in an oven (80 °C for 2 h). The control layer is peeled off the master and holes are punched as openings. The flow layer is made by spin-coating (2.0 krpm for 60 s) PDMS prepolymer on the mold and curing PDMS in an oven (80 °C for 1 h). The control layer is aligned and attached to the flow layer by the dipping-attaching method. The method is carried out by dipping the control layer into a thin film of PDMS prepolymer formed by spin-coating a 1/10 (w/w) PDMS prepolymer/cyclohexane solution at 3.0 krpm for 30 s onto a glass slide, followed by affixing the control layer onto the flow layer. The attachment is finally cured in an oven (80 °C for 2 h) and the thin film of PDMS serves as an adhesive layer between the two relatively thicker PDMS layers. The gold spots (50 nm thick on a 2 nm chromium layer) are deposited on a BK7 glass slide by thermal evaporation through a stainless-steel shadow mask. The uncoated area on the glass slide is covered by stamping a thin film of PDMS prepolymer, which is then cured in an oven (80 °C for 1 h). To complete the microfluidic device, the two-layer PDMS block is attached to the gold-deposited glass slide by the dipping-attaching method described earlier in this paragraph.

Running immunoassays in the microfluidic device

To achieve an immunoassay in the microfluidic device, reagent solutions are loaded into the reagent reservoirs and injected through the flow channels, causing immunocomplexes to appear on the gold spots (see Fig. 3). PBS buffer mixed with 0.1% (w/v) DDM (which we denote by DPBS) is employed for preventing physical adsorption of reagents to the PDMS flow channel walls during the immunoassay.[18] A home-made 16-output pressure controller is used to actuate valves and drive liquid flows. The manifold is controlled by a computer with LabVIEW software

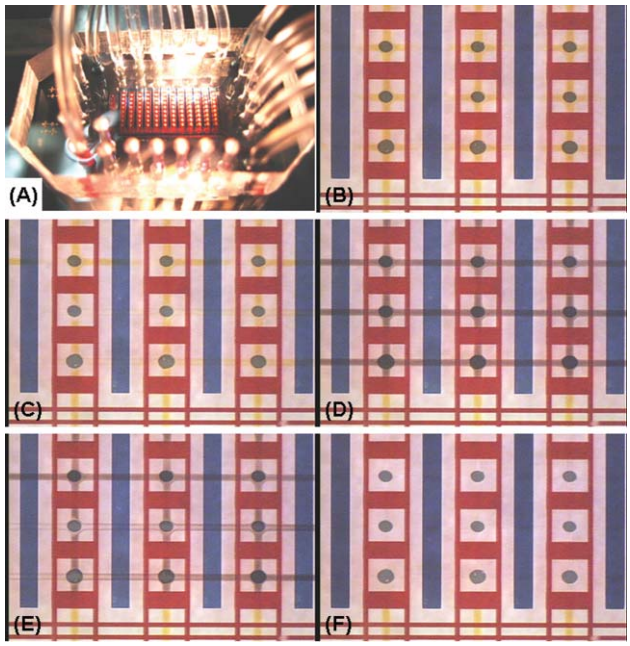

Fig. 3 (A) Picture of the microfluidic device while running an immunoassay. The tubes shown are connected to the pressure controller. (B)–(F) Illustration of the steps for carrying out immunoreactions in the microfluidic device, which are made visible using food coloring solutions. (B) Vertical reagent injection step: a reagent (yellow liquid) is injected into the flow channels to deliver the reagent to the gold spots. (C) & (E) Rinse steps: a washing buffer (clear liquid) is injected to rinse the gold spots. (D) Horizontal reagent injection step: a reagent (black liquid) is injected into the flow channels to deliver the reagent to the gold spots. (F) The channels in the microfluidic device are clear after the rinse step (E).

(National Instruments, Austin, TX, USA). It should be noted that the order of reagent injection is a matter of choice and need not follow what is shown in Fig. 3.

In order to detect the immunoreactions by SPR imaging, a setup is made to incorporate the microfluidic device into the optical pathway of the SPR imaging, as shown in Fig. 4. A collimated, p-polarized incoming light beam ($\lambda = 625$ nm) passes through a prism and illuminates the surface of the glass slide. The reflected light beam emerges from the prism and is collected by a home-built digital imaging device (not shown in Fig. 4). Two coaxial goniometers allow us to tune precisely the incident angle of the light onto the gold spots. The technical details of the SPR

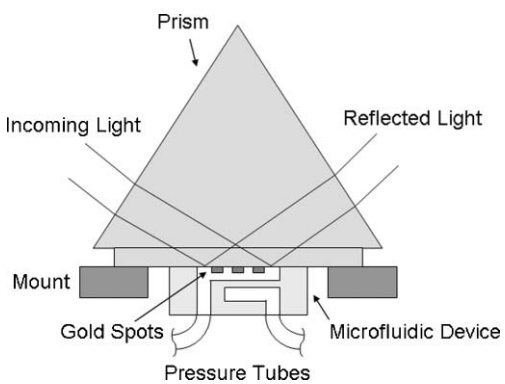

Fig. 4 Setup of the microfluidic device for SPR imaging.

This journal is © The Royal Society of Chemistry 2008

imaging setup are described elsewhere.[19] All immunoreactions taking place on the gold spots are monitored simultaneously in real-time, which provides kinetic information and facilitates throughput. In order to ensure the linearity of the SPR imaging signal, the working angle is adjusted to be ~1 degree smaller than the SPR minimum angle. During the immunoassay, both the microfluidic device and SPR imaging setup are at room temperature.

Processing of results

The digital images are numerically processed by MATLAB (The MathWorks, Natick, MA, USA) programs and graphically processed by ImageJ.[20] The center of each gold spot is manually selected and a certain region around the center is averaged to obtain the light reflectivity from the gold spot, which is called the SPR signal. The SPR signal of an immunoreaction subtracts the reference SPR signal (obtained from the gold spots not carrying out immunoreactions) to remove background. A kinetic curve of each immunoreaction is formed by plotting the SPR signal *versus* time. The immunoreaction result is obtained by subtracting the average of the starting signal points from the average of the ending signal points of the reagent injection period. To make calibration curves, the results are averaged for every four gold spots having replicated immunoreactions. Similarly, an image presenting the result of the immunoassay is made by subtracting the average of the beginning images from that of the ending images of the reagent injection period.

Results

Performance of the microfluidic device

The dipping-attaching method used to form the attachment between the PDMS block and the glass slide is essential to ensure the performance of the microfluidic device. The adhesive layer provides adequate bonding force between the PDMS block and glass slide, so that inter-flow-channel leakage is never found in running the immunoassays. Compared to the surface oxidation method usually employed for bonding PDMS to glass,[21] this method does not alter the PDMS surface.

The flow velocity in microfluidic flow channels is sensitive to surface properties because of the large surface-to-volume ratio. In the microfluidic device, the flow velocity usually varies under the same pressure. This may be caused by roughness of the PDMS channel walls. In the experiments, the flow velocity in the microfluidic device is controlled at about 15 mm s^{-1}, with a variation of about 1/3 fold. However, because the heterogeneous-phase reaction rate is related to the cubic root of flow velocity,[22] the immunoreaction kinetics is not significantly influenced. Therefore, the flow velocity is not taken into account in data analysis. For a flow velocity of 10 mm s^{-1}, the reagent consumption is 6 μL in 10 min in a flow channel of the microfluidic device, which is much smaller compared to the traditional microplate immunoassays.

One-step immunoassay

A one-step immunoassay is used to investigate the performance of the combined microfluidic device and the SPR imaging, in which biotin-BSA and anti-biotin Ab are used as the antigen–antibody pair. A group of biotin-BSA/BSA solutions with known concentrations are injected into the flow channels to prepare the surface-attached antigen by means of physical adsorption of biotin-BSA/BSA on the gold spots. Because biotin-BSA is competing with BSA during the physical adsorption, the surface density of biotin-BSA is related to the mixing ratio. To carry out immunoreactions, a group of anti-biotin Ab solutions with known concentrations are then injected into the flow channels. They form immunocomplexes with the immobilized biotin-BSA. The kinetics of the immunocomplex formation, monitored by SPR, is related to both the surface density of the biotin-BSA and the concentration of the anti-biotin Ab.

Fig. 5A shows the image before injection of the antibody solutions and Fig. 5B shows the subtracted image before and after injection of the antibody solutions. Because the surface density of biotin-BSA increases from top to bottom and the concentration of the anti-biotin BSA solutions increases from left to right, the surface density of immunocomplex ascends from top-left toward bottom-right, as shown in Fig. 5B. The left most two vertical channels are injected with pure buffer so no immunoreaction is expected. These serve as reference signals to

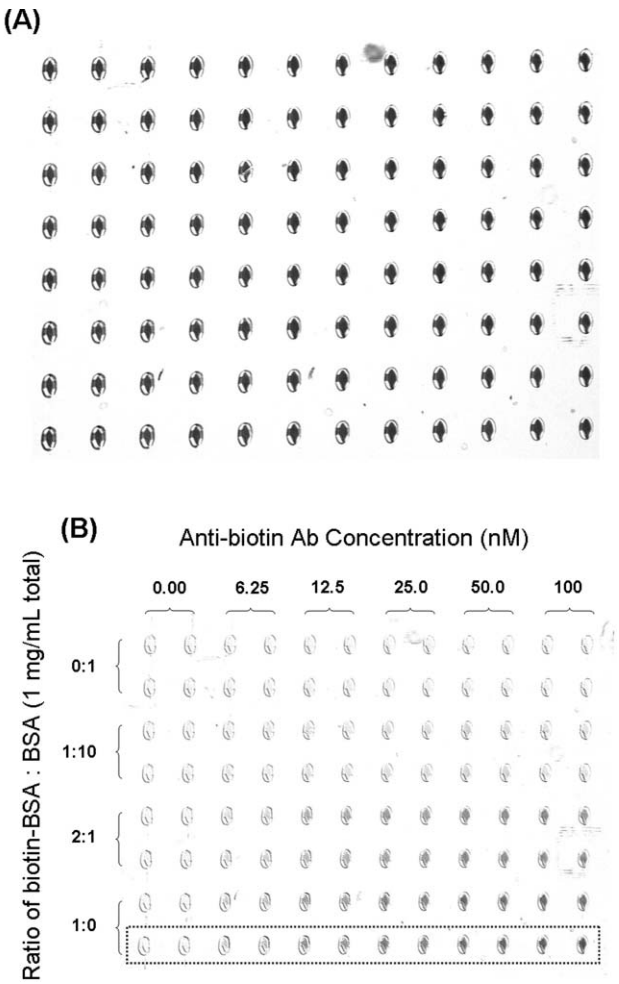

Fig. 5 (A) Starting SPR image of the gold spots covered by biotin-BSA layer, and (B) the difference of the SPR images obtained after and before the one-step immunoreaction. The dashed box outlines those spots that will be used in Fig. 6A.

remove any artifacts from the temperature or pressure variation during the sample injection.

With real-time SPR imaging, the binding kinetics of each immunoreaction is recorded. Fig. 6A shows the kinetic curves of anti-biotin Ab binding to biotin-BSA taking place on the gold spots indicated in Fig. 5B. The curve is constructed by taking the average of the two replicated immunoreactions. From the kinetic curves it is found that the SPR signals are easily distinguishable at about 10 min, indicating the capability of real-time sample quantitation. Within about 40 min, the SPR signal shows biphasic kinetics of immunoreactions and is still yet to reach equilibrium. Therefore, it is important to establish a calibration curve in every quantitation experiment, even though the SPR imaging conditions remain the same. Moreover, SPR signals are sensitive to both surface refractive change by molecule binding and bulk refractive index change by pressure or temperature change. Therefore, SPR signal artifacts are observed at the beginning of the kinetic curves when the valves are opened to allow liquid flows in the microfluidic device. This artifact may be completely eliminated by proper referencing[23] or by surface patterning.[24]

Fig. 6B shows the dose-response curves established from the immunoreaction results averaged from every four replicated immunoreactions. Each dose-response curve reaches saturation at a certain concentration of anti-biotin Ab, which may be explained by the limited binding capacity of biotin-BSA immobilized on the gold spots. The uncertainty associated with each point is the standard deviation of the four replicated immunoreactions.

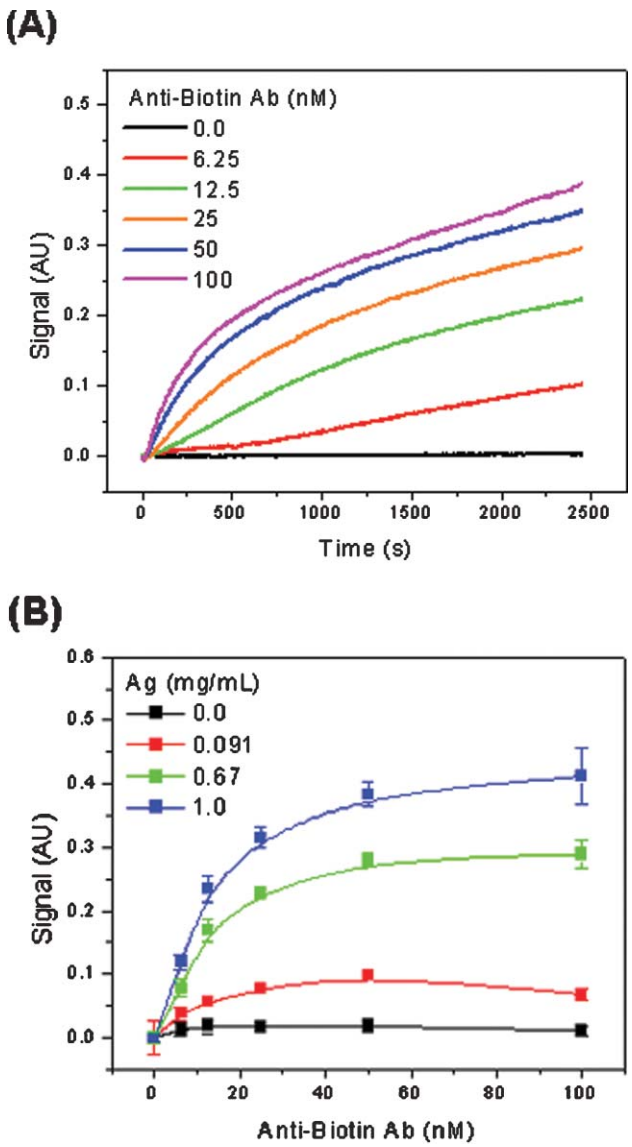

Fig. 6 (A) Kinetic curves of anti-biotin Ab binding to surface-attached biotin-BSA on the gold spots outlined in Fig. 5B. Every two gold spots with replicated immunoreactions are averaged. (B) Dose-response curves obtained by averaging the results of replicated immunoreactions on every four gold spots.

Two-step immunoassay

A real sample usually has multiple components that could interfere with the immunoassay. Moreover, the component of

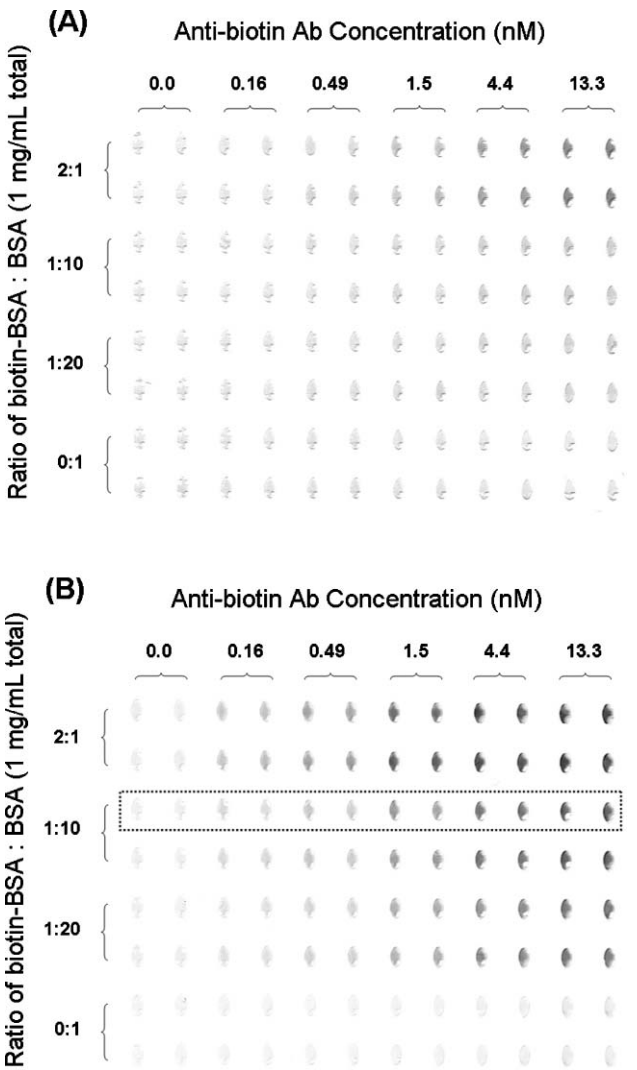

Fig. 7 (A) The difference of images before and after step 1 of the two-step immunoassay. (B) The difference of images before and after step 2 of the two-step immunoassay. The dashed box outlines those spots that will be used in Fig. 8C.

This journal is © The Royal Society of Chemistry 2008

interest is often present in low concentration. Consequently, we seek a means of enhancing the specificity and sensitivity of our procedure. For this purpose, we add an additional step to bring about signal amplification. We add a secondary antibody that has been labeled with one or more gold nanoparticles.[25,26] In the particular model system we are examining, we use gold-nanoparticle-labeled anti-goat IgG antibody (AuNP-Ab), which is delivered to the gold spots as a final step. It specifically binds to the anti-biotin Ab to form a three-member immunocomplex and generates a strong SPR signal from the high refractive-index gold nanoparticles. Compared to the one-step immunoassay, the surface density of the anti-biotin Ab is obtained by quantifying that of the three-member immunocomplex. Because the kinetics of the three-member immunocomplex formation is related to both the surface density of the anti-biotin Ab and the concentration of the AuNP-Ab, monitoring the second immunoreaction step achieves indirect quantitation of the anti-biotin Ab brought in by the first immunoreaction step.

Fig. 7A and 7B show the imaging results in steps 1 and 2 of the immunoassay, respectively. Step 1 repeats the immunoreactions in the one-step immunoassay but with decreased biotin-BSA and anti-biotin Ab concentrations. The left most two vertical channels are injected with pure buffer to serve as reference signals. The bottom most two horizontal channels containing the gold spots fully covered by BSA can also be used as reference signals because no immunoreaction is expected in this particular experiment. Fig. 8A shows dose-response curves established by the results of the immunoreactions in step 1. We defined the limit of detection as a signal-to-noise ratio of three where we compare to the blank samples (two reference channels shown on the left most part plus two shown on the bottom most part of Fig. 7A and 7B). With this definition, it is found that the limits of detection are about 0.21 nM and 0.57 nM on the gold spots covered by biotin-BSA/BSA 2 : 1 and biotin-BSA/BSA 1/10, respectively.

In step 2, a solution of AuNP-Ab 1/20 (v/v) in DPBS is injected through the horizontal flow channels. The antibody recognizes and binds to the anti-biotin Ab immobilized on the gold spots. Fig. 8B shows the dose-response curves obtained by the results of the immunoreactions in step 2, and Fig. 8C

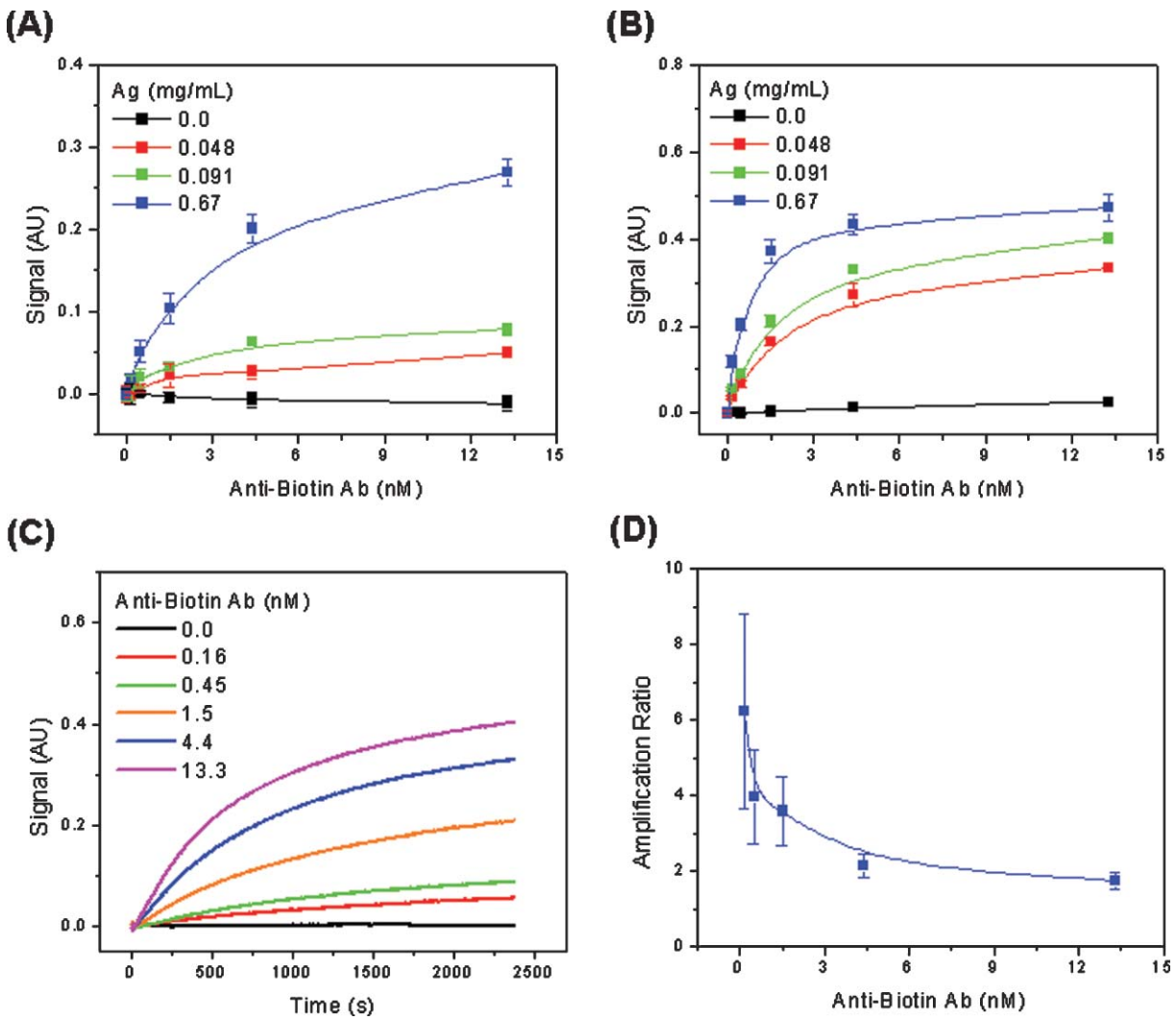

Fig. 8 (A) Dose-response curves obtained as the average of the replicated immunoreactions on every four gold spots after step 1. (B) Same as (A) after step 2. (C) Kinetic curves of AuNP-Ab binding to the immunocomplex formed on the gold spots, outlined in Fig. 7B. (D) Amplification ratios between the results of step 1 and step 2 from the gold spots covered by biotin-BSA/BSA in the ratio 2 : 1.

shows the corresponding kinetic curves obtained from the gold spots outlined in Fig. 7B. The signal amplification step extends the limits of detection to about 38 pM and 82 pM on the gold spots covered by biotin-BSA/BSA 2 : 1 and biotin-BSA/BSA 1/10. Compared to those in step 1, the sensitivity has been significantly enhanced. These results demonstrate the potential to apply the combined microfluidic device and SPR imaging readout to quantify real samples, where the components of interest are usually present in low concentrations.

Fig. 8D shows amplification ratios calculated by dividing the results of step 2 by step 1 for the gold spots covered by biotin-BSA/BSA in the ratio 2 : 1. The amplification ratio decreases as the anti-biotin Ab concentration increases. This behavior indicates that the lower surface density of the primary antibody tends to have a higher binding efficiency for the secondary antibody, which can be explained by the more efficient binding of the secondary antibody when the primary antibody is not crowded.[27] The amplification ratio shown in Fig. 8D has a maximum value of about 6.5; however, the amplification ratio would be still higher if we compared the gold spots covered with a lower concentration of anti-biotin Ab.

Discussion

The microfluidic device shows excellent performance as a microscale platform for immunoreactions. Beyond that, the microfluidic device presents a model to interface a surface-probing spectroscopic technique with small instrument size, low reagent consumption, and system automation, which may have potential value for point-of-care medical applications.

The combined microfluidic device and SPR imaging readout provide excellent sensitivity and efficiency for carrying out immunoassays. This prototype system is the first of its kind. Presently, it approaches but does not attain the sensitivity of the best ELISA results, which is typically at the level of picomolar, but it is appreciably faster with much less sample consumption. The results are also comparable to the fluidics-based flow injection analysis immunoassays,[28] which are renowned for high speed and sensitivity but usually not as easy for high throughput as microfluidic devices. Some aspects of the microfluidic device can be optimized to improve the performance of the system. The gold spots may be chemically modified to increase the activity of the antigen or antibody that is first added. A possible way to accomplish this task is forming a self-assembled monolayer on the gold spots before the microfluidic device is assembled. Moreover, the liquid flow rate in a channel is influenced by structural defects or the chemical environment of the channel walls. The liquid flows may be driven by a peristaltic pump providing constant-rate instead of constant-force liquid flows. In this way, the flow rate would be kept exactly the same in all flow channels. With further improvements we anticipate that the combination of microfluidic sample manipulation and surface plasmon resonance readout may have many useful applications to real-world problems.

References

1 R. M. Lequin, *Clin. Chem.*, 2005, **51**, 2415–2418.
2 A. Voller, A. Bartlett and D. E. Bidwell, *J. Clin. Pathol.*, 1978, **31**, 507–520.
3 T. Bravman, V. Bronner, K. Lavie, A. Notcovich, G. A. Papalia and D. G. Myszka, *Anal. Biochem.*, 2006, **358**, 281–288.
4 S. K. Sia, V. Linder, B. A. Parviz, A. Siegel and G. M. Whitesides, *Angew. Chem., Int. Ed.*, 2004, **43**, 498–502.
5 E. Eteshola and D. Leckband, *Sens. Actuators, B*, 2001, **72**, 129–133.
6 F. Y. H. Lin, M. Sabri, D. Erickson, J. Alirezaie, D. Q. Li and P. M. Sherman, *Analyst*, 2004, **129**, 823–828.
7 R. Kurita, Y. Yokota, Y. Sato, F. Mizutani and O. Niwa, *Anal. Chem.*, 2006, **78**, 5525–5531.
8 N. H. Chiem and D. J. Harrison, *Clin. Chem.*, 1998, **44**, 591–598.
9 K. Sato, M. Yamanaka, H. Takahashi, M. Tokeshi, H. Kimura and T. Kitamori, *Electrophoresis*, 2002, **23**, 734–739.
10 G. J. Wegner, A. W. Wark, H. J. Lee, E. Codner, T. Saeki, S. P. Fang and R. M. Corn, *Anal. Chem.*, 2004, **76**, 5677–5684.
11 E. Fu, T. Chinowsky, K. Nelson, K. Johnston, T. Edwards, K. Helton, M. Grow, J. W. Miller and P. Yager, *Ann. N. Y. Acad. Sci.*, 2007, **1098**, 335–344.
12 J. S. Rossier and H. H. Girault, *Lab Chip*, 2001, **1**, 153–157.
13 S. Lai, S. Wang, J. Luo, L. J. Lee, S. Yang and M. J. Madou, *Anal. Chem.*, 2004, **76**, 1832–1837.
14 K. Lee, Y. Su, S. Chen, F. Tseng and G. Lee, *Biosens. Bioelectron.*, 2007, **23**, 466–472.
15 E. Yeatman and E. A. Ash, *Electron. Lett*, 1987, **23**, 1091–1092.
16 B. Rothenhaüsler and W. Knoll, *Nature*, 1988, **332**, 615–616.
17 H. Wu, B. Huang and R. N. Zare, *Lab Chip*, 2005, **5**, 1393–1398.
18 B. Huang, H. K. Wu, S. Kim and R. N. Zare, *Lab Chip*, 2005, **5**, 1005–1007.
19 F. Yu, Y. Luo, L. M. Leslie, Y. M. Soto, K. E. Mach, J. C. Liao and R. N. Zare, unpublished work.
20 See http://rsb.info.nih.gov/ij/.
21 S. Bhattacharya, A. Datta, J. M. Berg and S. Gangopadhyay, *J. Microelectromech. Syst.*, 2005, **14**, 590–597.
22 R. F. Probstein, *Physicochemical Hydrodynamics*, 2nd edn, Wiley-Interscience, Cambridge, MA, 2003.
23 H. B. Lu, J. Homola, C. T. Campbell, G. G. Nenninger, S. S. Yee and B. D. Ratner, *Sens. Actuators, B*, 2001, **74**, 91–99.
24 F. Yu and W. Knoll, *Anal. Chem.*, 2004, **76**, 1971–1975.
25 S. Kubitschko, J. Spinke, T. Bruckner, S. Pohl and N. Oranth, *Anal. Biochem.*, 1997, **253**, 112–122.
26 L. He, M. D. Musick, S. R. Nicewarner, F. G. Salinas, S. J. Benkovic, M. J. Natan and C. D. Keating, *J. Am. Chem. Soc.*, 2000, **122**, 9071–9077.
27 F. Yu, D. Yao and W. Knoll, *Anal. Chem.*, 2003, **75**, 2610–2617.
28 Y. Fintschenko and G. S. Wilson, *Microchim. Acta*, 1998, **129**, 7–18.

 This journal is © The Royal Society of Chemistry 2008